Hindawi Publishing Corporation
Abstract and Applied Analysis
Volume 2014, Article ID 968017, 10 pages
http://dx.doi.org/10.1155/2014/968017

Research Article

Observer Based Traction/Braking Control Design for High Speed Trains Considering Adhesion Nonlinearity

Wenchuan Cai,[1] Wenhao Liao,[1] Danyong Li,[1] and Yongduan Song[1,2]

[1] *School of Electronic and Information Engineering, Beijing Jiaotong University, Beijing 100044, China*
[2] *School of Automation, Chongqing University, Chongqing 400044, China*

Correspondence should be addressed to Yongduan Song; ydsong@cqu.edu.cn

Received 18 January 2014; Accepted 28 January 2014; Published 6 March 2014

Academic Editor: Peng Shi

Train traction/braking control, one of the key enabling technologies for automatic train operation, literally takes its action through adhesion force. However, adhesion coefficient of high speed train (HST) is uncertain in general because it varies with wheel-rail surface condition and running speed; thus, it is extremely difficult to be measured, which makes traction/braking control design and implementation of HSTs greatly challenging. In this work, force observers are applied to estimate the adhesion force or/and the resistance, based on which simple traction/braking control schemes are established under the consideration of actual wheel-rail adhesion condition. It is shown that the proposed controllers have simple structure and can be easily implemented from real applications. Numerical simulation also validates the effectiveness of the proposed control scheme.

1. Introduction

With rapid development of high speed railway, the railway transport system brings great convenience to our daily life and changes our travel habit. However, high speed operation leads to great challenges for train traffic safety. ATO (automatic train operation) is one of the key technologies to ensure the train traffic safety whose performance strictly relays on reliability of braking and traction systems and also is affected by line conditions (slope, curve, tunnel, etc.), the speed limit, train weight, weather conditions, and so forth. Advanced control for ATO system plays an important role in maintaining safe, reliable, and cost-effective operation of HSTs.

Early researches on ATO of trains have been mainly focused on optimal operation to ensure punctuality, precision parking, passenger comfort, energy conservation, and so on [1–3], where largely oversimplified models in the form of either linearized or decoupled models normally with nonlinear term disregarded are employed. Such approximation apparently limits the region of train operation where the controller is valid, which makes it difficult for these methods to maintain satisfied performance as the traveling speed increases, especially for ATO design of HSTs. For this reason, some nonlinear modeling and control methods for HSTs appeared in recent years.

For high-performance control of a high speed train in terms of tracking accuracy, stability, and robustness, crucial factors to be usually addressed in ATO control design include in-train forces, aerodynamic resistance, input nonlinearities arisen from traction/braking notches, disturbing forces, and actuation and braking faults due to varying railway conditions (such as curvature, tunnel, and ramp). For example, the work [4] developed a multidimensional cascade model for HSTs, where the basic and aerodynamic resistances and in-train forces were considered. In [5], a multimass and single coordinate dynamic model for HSTs was constructed, where coupling effects between adjacent vehicles can be reflected, but the immeasurable in-train forces are cancelled out so as to simplify control design and analysis. Note that the influence of aerodynamic resistance on the train's dynamic behavior becomes increasingly significant as the train speed increases [6, 7]; thus, it has also attracted considerable attention and nonlinear control methods (e.g., robust adaptive control algorithms [5], neuroadaptive fault-tolerant control algorithms [8, 9], and adaptive backstepping methods [10, 11]) were developed to ensure high precision speed and position tracking under various factors such as resistive friction and aerodynamic drag forces, interactive impacts among the vehicles, nonlinear traction/braking notches inherent in train systems,

actuator failures, or/and uncertain impacts of in-train forces in the system.

It is worth noting that most existing control methods for ATO system only make efforts to find proper traction/braking force commands, and very few accounts for wheel-rail adhesion constraints in control design of ATO. It is known that the adhesive coefficient exhibits highly complex and nonlinear behavior, especially in presence of degraded adhesion and large sliding between the contact surfaces due to external unknown contaminants [12], such that an accurate adhesion model is extremely difficult, if not impossible, to predetermine [13], which possibly degrades the performance of most traction/braking force command based approaches, or even destroys their stability. To deal with this problem, we first introduce an adhesive force observer to realize the desired traction/braking force command, which originates from the disturbance observer widely used for motion control in industry applications [14–18]. Motivated by such idea, several disturbance observers are designed in this work, based on which simple traction/braking control schemes are established under the consideration of actual wheel-rail adhesion condition, without need of precise information of adhesion conditions or/and resistances.

The rest of this paper is organized as follows. In Section 2, a nonlinear dynamic model considering adhesion constraints is developed. Section 3 describes the complete observer and control structures, respectively, and convergence issue is established via formative mathematical analysis. Several numerical simulations on a train similar to CRH3 under various driving conditions are conducted in Section 4 to visualize the efficacy of the method. Section 5 concludes this paper.

2. Dynamic Modeling of HSTs

2.1. Longitudinal Dynamics of Train Body. Consider an HST with n vehicles connected by $n-1$ nonlinear and elastic couplers and draft gears, which are equipped with p traction motors or braking units in the presence of both notch effects and adherence-antiskid constraints. By [12], the multiple point-mass model that accounts for in-train forces, uncertain resistive forces can be derived as follows:

$$m_i\ddot{x}_i = F_{ai} + F_{\mathrm{in}_{i-1}} - F_{\mathrm{in}_i} + F_{ri} \quad (i = 1, 2, \ldots, n), \tag{1}$$

where m_i is the mass of the ith vehicle which might not be accurately available due to variation of passengers and loads; x_i is the position of the ith vehicle; F_{ai} represents either the traction force ($F_{ai} = 0$ if the ith vehicle is a carriage) or braking force; f_{in_i} is in-train force between the ith and the $(i+1)$th vehicle, which is essentially a nonlinear and uncertain function of states $x_i, x_{i+1}, \dot{x}_i, \dot{x}_{i+1}$ and the parameter of the ith coupler-draft gear $\mathbf{p}_i$; that is, $F_{\mathrm{in}_i} = F_{\mathrm{in}_i}(x_i, x_{i+1}, \dot{x}_i, \dot{x}_{i+1}, \mathbf{p}_i)$ (note that $F_{\mathrm{in}_0} = F_{\mathrm{in}_p} = 0$ as there is no in-train force at the front of the first vehicle and the end of the last one); F_{ri} is the resistive force for each vehicle, taking the following form:

$$F_{ri} = a_{0i} + a_{1i}\dot{x}_i + a_{2i}\dot{x}_i^2 + o_i\left(x_i, \dot{x}_i\right) + F_{\mathrm{rr}i}. \tag{2}$$

Here a_{0i}, a_{1i}, and a_{2i} are the resistive coefficients for the ith vehicle; $F_{\mathrm{rr}i}$ is the rail resistance acting on the ith vehicle, such as the ramp resistance due to the track slope, the curve resistance due to railway curvature, and the tunnel resistance; and $o_i(x_i, \dot{x}_i)$ represents a lumped nonparameterized term with respect to $x_i, \dot{x}_i$.

Remark 1. It is worth noting that the model F_{ri} given in (2) without the term $o_i(x_i, \dot{x}_i)$ is already acceptable to express the resistance for most normal speed trains. However, the resistance acted on the vehicle of HSTs exhibits more highly nonlinear variation, which thus becomes more difficult to be linearly parameterized. How to compensate such nonparameterized resistance is a very important and challenging issue for traction/braking control of HSTs.

To establish the train dynamics, we first need to address the impact of the in-train forces. As such forces are difficult to model, dealing with such impact directly is extremely challenging. It is interesting to note that, however, the in-train forces f_{in_i} obey the "action and reaction" rule; thus, these forces always appear in opposite directions between any two vehicles; regardless of whether the connection is rigid or elastic, this condition motivates the use of the summation of (1) on both sides to get the following multiple-point-mass and single-coordinate traction model [5], in which the in-train forces are naturally canceled out (because $\sum_{i=1}^{n}(F_{\mathrm{in}_{i-1}} - F_{\mathrm{in}_i}) = 0$):

$$m\ddot{x} = F_a - F_d(\cdot) \tag{3}$$

with

$$\begin{aligned} F_d(\cdot) = {} & \left(\sum_{i=1}^{n} a_{0i}\right) + \left(\sum_{i=1}^{n} a_{1i}\right)\dot{x} + \left(\sum_{i=1}^{n} a_{2i}\right)\dot{x}^2 \\ & + \sum_{i=1}^{n}\left[m_i\left(\ddot{x}_i - \ddot{x}\right) + o_i\left(x_i, \dot{x}_i\right) + F_{ri}\right] \\ & + \sum_{i=1}^{n}\left[a_{1i}\left(\dot{x}_i - \dot{x}\right) + a_{2i}\left(\dot{x}_i^2 - \dot{x}^2\right)\right], \end{aligned} \tag{4}$$

where $m = \sum_{i=1}^{n} m_i$ is the total mass of the train, $F_a = \sum_{i=1}^{p} F_{ai}$ represents the total traction/braking force; x, $\dot{x}$, and $\ddot{x}$ are the reference (average) position, velocity, and acceleration of the train.

Remark 2. Apparently, the model considered in (3) is able to characterize the dynamic behavior of a train more precisely in comparison with the single point-mass model or the multiple point-mass model with linear approximation commonly used. However, it should be stressed that it is generally difficult to measure or model the in-train forces involved in the system due to the nonlinear and elastic nature of the couplers connecting the vehicles. In most existing works such in-train forces are either ignored or approximated with a linear model [2].

2.2. Problem of Practical Operation of HSTs. Based on the dynamic model (3), the traction control problem can be stated as follows. Let x^*, $\dot{x}^*$, and $\ddot{x}^*$ be the desired displacement, velocity, and acceleration of the reference vehicle,

which are all assumed to be smooth and bounded. Define a tracking position error and a filtered error variable as follows:

$$e = x - x^*, \tag{5}$$

$$s = \dot{e} + \beta e. \tag{6}$$

Thus, the error dynamics of traction/braking operation is obtained from (3) and (6) as

$$m\dot{s} = F_a - F_d(\cdot) - m\ddot{x}^* + \beta\dot{e} \tag{7}$$

which together with (13) implies that if the given drive torque T_{mi} can ensure $s \to 0$ as $t \to \infty$, then the objective of traction/braking control in the sense that $e, \dot{e} \to 0$ as $t \to \infty$ is achieved. Thus, the left problem of traction/braking control considering adhesion limit is to design a proper T_{mi} to achieve $s \to 0$ as $t \to \infty$.

Most existing methods for ATO of HSTs are based on either direct cancellation of all the nonlinearities or indirect compensation for the nonlinearities and uncertainties in the system. Namely, the adhesive force in (7) is generated in form of

$$F_a = -k_0 s + m\ddot{x}^* - \beta\dot{e} + F_d(\cdot) \tag{8}$$

or

$$F_a = -k_0 s + m\ddot{x}^* - \beta\dot{e} + \widehat{F}_d(\cdot), \tag{9}$$

where $\widehat{F}_d(\cdot)$ represents the estimation of the complex term $F_d(\cdot)$.

It is worth noting that if $F_d(\cdot)$ is precisely available for control design, the autopilot strategy (8) represents the well-known model based nonlinear inverse control. However, as $F_d(\cdot)$ in (4) lumps all the nonlinear and uncertain impact on the train dynamics during its operation, the direct cancellation method, although theoretically attractive, is impractical and undesirable because it not only demands quite complicated on-line computing, but also incomputable one.

The estimation based strategy (9) is built upon estimating and compensating the nonlinear and uncertain $F_d(\cdot)$. Such estimation is normally done by regressor (linear parametric decomposition) based method [5], learning based method (i.e., NN, fuzzy) [8, 9, 19], or other methods (i.e., VSC, robust adaptive, etc.) [5, 10, 11, 20]. As a large number of on-line updating/learning of weights are involved, this method demands significant amount of on-line computation; thus, it is not an ideal choice for HSTs.

Moreover, the signal as given by (8) or (9) only represents the adhesion force command, rather than the actual adhesion force generated by the wheel-rail adhesion system, involving nonlinearity and uncertainty, so that the effectiveness of (8) or (9) is based on the assumption that F_a can be perfectly realized in the wheel-rail system. However, the mechanism of actual adhesion process is very complicated and varies with wheel-rail surface conditions; thus, it involves nonlinearity and uncertainty in general. Therefore, it is necessary to take the wheel-rail adhesion into account in control design or control implementation for HSTs.

2.3. Property of Wheel-Rail Adhesion. It is known that the actual traction/braking force in (3) is generated indirectly though the wheel-rail adhesion system as

$$F_{ai} = \mu_i(\lambda_i, v_i) m_i g_0, \tag{10}$$

where g_0 is the gravity constant, $\mu_i(\lambda_i, v_i)$ is the adhesive coefficient, which is a nonlinear function with respect to the train body velocity $v_i = \dot{x}_i$ and the slip ratio between the wheel and the rail λ_i, and λ_i is defined as

$$\lambda_i = \frac{\omega_i R - v_i}{\max(\omega_i R, v_i)} \tag{11}$$

in which ω_i is the angular velocity of the ith wheel, which is characterized as

$$J\dot{\omega}_i = T_{mi} - F_{ai} R, \tag{12}$$

where J is the moment of inertia of the driving system (including wheels, transmission, and driving motor), R is the wheel radius, and τ_{mi} is the control torque of the ith driving motor or braking unit.

Note that for most adhesion control it is assumed that the adhesive coefficient only depends on the slip ratio λ_i, which is modeled as [12]

$$\mu_i(\lambda_i, v_i) = \mu_i(\lambda_i) = b_1(1 - \exp(-b_2\lambda_i)) - \frac{\lambda_i}{b_3}, \tag{13}$$

where different coefficients (b_1, b_2, b_3) represent different adhesion conditions. It is worth noting that as the train speed increases, the effect of the aerodynamic lift due to increasing speed on the adhesive coefficient cannot be ignored because the increasing aerodynamic lift acted on the train body reduces the normal force between the wheel and the rail surfaces; thus, it decreases the adhesive force according to (8). To describe such property, the adhesive coefficient for HSTs can be expressed as

$$\mu_i(\lambda_i, v_i) = \frac{\mu_{i\max}(v_i)}{\mu_{\max}(0)} \mu_i(\lambda_i), \tag{14}$$

where $\mu_{i\max}(v_i)$ represents the peak value of μ_i for a given train speed v_i, which is a nonlinear function relative to v_i [12]

$$\mu_{i\max}(v_i) = c_1 + \frac{c_2}{c_3 + v_i}, \tag{15}$$

where c_1, c_2, and c_3 are some constants depending on the wheel-rail surface condition, and thus the actual adhesive coefficient. The actual adhesive coefficient $\mu_i(\lambda_i, v_i)$ is illustrated in Figure 1, where $\mu_i(\lambda_i, v_i)$ decreases as v_i increases but λ_i does not change. Obviously, the adhesive coefficient of HTS given in (11) exhibits highly nonlinear and is more complicated than that of the medium-low speed train as given by (10). Hence, it is greatly challenging to design the actual control torque T_{mi} for the system (12) to ensure that the desired adhesive force is always obtained for ATO of HSTs.

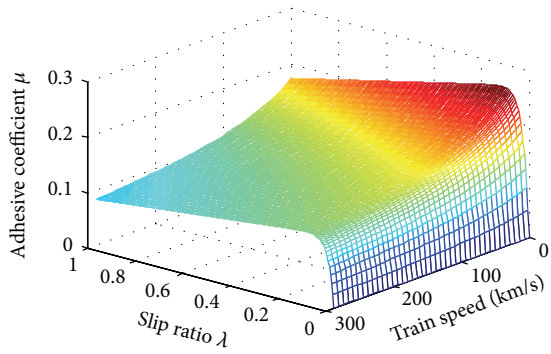

FIGURE 1: Adhesion property of HSTs.

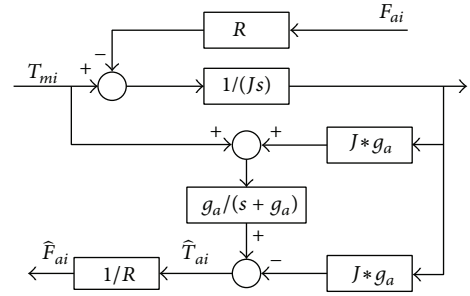

FIGURE 2: Adhesion force observer ($\widehat{F}_{ai}$).

3. Traction/Braking Control with Adhesion Nonlinearity

To consider nonlinearity of the wheel-rail system in traction/braking control design, a direct idea to design T_{mi} is to take the derivative of the dynamic system (3) to extract $\dot{\omega}_i$ from the adhesive force (8) so as to get a third-order dynamic system:

$$\begin{aligned} m\dddot{x} &= \sum_{i=1}^{m}\left(\frac{\partial F_{ai}}{\partial \omega_i}\dot{\omega}_i + \frac{\partial F_{ai}}{\partial v_i}\dot{v}_i\right) - \dot{F}_d(\cdot) \\ &= \frac{1}{J}\sum_{i=1}^{m}\frac{\partial F_{ai}}{\partial \omega_i}\left(T_{mi} + F_{ai}R\right) - \dot{F}_d(\cdot) + \sum_{i=1}^{m}\frac{\partial F_{ai}}{\partial v_i}\dot{v}_i \end{aligned} \tag{16}$$

which has an affine input T_{mi}, so that most nonlinear control methods can be applied to determine a proper T_{mi} to ensure $e, \dot{e} \to 0$ as $t \to \infty$. However, this method is not preferred for practical applications since it is very difficult to derive the control gain $\partial F_{ai}/\partial \omega_i$ from a nonlinear and uncertain adhesive force curve (10); acceleration of the train body is required for control design; both the nonlinear and uncertain adhesive force F_{ai} and the derivative of complex resistance $\dot{F}_d$ are needed to compensate simultaneously, which are the possible reason that few methods take the dynamics and nonlinearity of the wheel system into account of control design, especially investigated from the dynamic system (16). To deal with these problems, several simple practical approaches without detailed information of wheel-rail adhesion system are presented in what follows.

3.1. Adhesive Force Control Design. If the adhesive force command F_{ai}^{cmd} of each driving is already obtained as given by (8) or (9), which is proven to be effective without considering the wheel-rail adhesion, then to apply these existing results to more practical cases, one only needs to design the driving torque T_{mi} to ensure that the actual adhesive force F_a strictly tracks F_a^{cmd}, according the wheel dynamic system (12). Note that if the actual adhesive force F_{ai} is measureable, then a force-feedback control method can be designed as

$$T_{mi} = k_a\left(F_{ai}^{\text{cmd}} - F_{ai}\right) + F_{ai}R, \tag{17}$$

where $k_a > 0$ is a constant parameter. Substituting it into (12) leads to $J\dot{\omega}_i = k_a(F_{ai}^{\text{cmd}} - F_{ai})$, which implies that once the wheel system becomes steady, $F_{ai}^{\text{cmd}} \to F_{ai}$ is achieved such that the overall objective of traction/braking control is realized. For real application, the adhesion force F_{ai} in (17), even though is very complex, can be estimated as the observer shown in Figure 2, from which together with (12) we have

$$\begin{aligned} \widehat{F}_{ai} &= \frac{1}{R}\left[\frac{g_a}{s+g_a}\left(T_{mi} + g_a J\omega_i\right) - g_a J\omega_i\right] \\ &= \frac{1}{R}\left[\frac{g_a}{s+g_a}\left(T_{mi} - J\dot{\omega}_i\right)\right] = \frac{g_a}{s+g_a}F_{ai}, \end{aligned} \tag{18}$$

where $g_a > 0$ represents the cutoff frequency of the observer. It can be seen that $\widehat{F}_{ai} \to F_{ai}$ as long as g_a is larger than the bandwidth of the driving wheel system, and even though the proposed observer involves estimation of $\dot{\omega}_i$, it does not need to measure wheel acceleration $\dot{\omega}_i$ and thus is feasible from the point view of engineering implementation. Consequently, the actual control is

$$T_{mi} = k_a\left(F_{ai}^{\text{cmd}} - \widehat{F}_{ai}\right) + \widehat{F}_{ai}R. \tag{19}$$

Remark 3. By applying the force-feedback control technology, not only most existing methods for train ATO can be realized by (19), but also the wheel-rail dynamics and nonlinearity is considered explicitly without complicated analysis and estimation of the wheel-rail adhesive force. However, even without considering the wheel-rail adhesion, it is still not easy to design the adhesive force command F_{ai}^{cmd} from (7) to cope with the F_d given by (4), in which, for example, the in-train forces are difficult to measure or model in general due to the nonlinear and elastic nature of the couplers connecting the vehicles. For this reason, a double observer based control method is presented as follows.

3.2. Double Observer Based Method. It can be observed that if the resistance F_d is estimated precisely, then the ideal control (8) can be applied to generated the adhesive force command F_{ai}^{cmd} in (19), such that a more practical is established based on (19).

Motivated by this observation, a double observer based control method is developed as

$$F_{ai}^{\text{cmd}} = \frac{1}{p_i}F_a^{\text{cmd}} = \frac{1}{p_i}\left(-k_0 s + m\ddot{x}^* - \beta\dot{e} + \widehat{F}_d\right), \tag{20}$$

$$T_{mi} = k_a\left(F_{ai}^{\text{cmd}} - \widehat{F}_{ai}\right) + \widehat{F}_{ai}R, \tag{21}$$

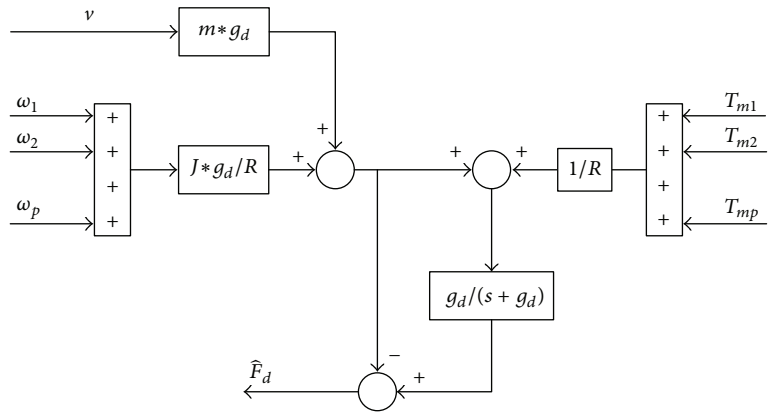

FIGURE 3: Resistance observer ($\widehat{F}_d$).

where $\sum_i^p 1/p_i = 1$, the estimated adhesive force $\widehat{F}_{ai}$ is obtained by the observer given in Figure 2, and the resistance $\widehat{F}_d$ is achieved by the observer as constructed in Figure 3; obviously this is practically feasible since it only uses measurable variables (i.e., angular velocity of all driving wheel, velocity of the train body, and control torques acted on all driving wheels).

Based on the structure given in Figure 3, one can infer that

$$\begin{aligned}\widehat{F}_d &= \frac{g_d}{s+g_d}\left[g_d m v + \frac{1}{R}\sum_{i=1}^{p}\left(T_{mi} + g_d J\omega_i\right)\right] \\ &\quad - g_d\left(mv + \frac{J}{R}\sum_{i=1}^{p}\omega_i\right) \\ &= \frac{g_d}{s+g_d}\left[\frac{1}{R}\sum_{i=1}^{p}T_{mi} - m\ddot{x} - \frac{J}{R}\sum_{i=1}^{p}\dot{\omega}_i\right]\end{aligned} \tag{22}$$

and from (3) and (12), the resistance F_r can be expressed as

$$F_d = \frac{1}{R}\sum_{i=1}^{p}T_{mi} - m\ddot{x} - \frac{J}{R}\sum_{i=1}^{p}\dot{\omega}_i. \tag{23}$$

Thus, substituting (23) into (22), we have

$$\widehat{F}_d = \frac{g_d}{s+g_d}F_d, \tag{24}$$

where $g_d > 0$ represents the cutoff frequency of the observer, so that $\widehat{F}_d \to F_d$ is ensured as long as g_d is larger than the bandwidth of the overall dynamic system.

It is worth noting that if $\widehat{F}_r = F_r$ and $\widehat{F}_{ai} = F_{ai}$ are already achieved, then from (21) and (20) one infers that

$$F_a = pF_{ai}^{\mathrm{cmd}} = -k_0 s + m\ddot{x}^* - \beta\dot{e} + F_r \tag{25}$$

substituting it into (7) leads to $m\dot{s}+k_0 s = 0$, which implies that s converges to zero exponentially, so that asymptotically stable traction/braking control is achieved (i.e., $e, \dot{e} \to 0$ as $t \to \infty$). However, for real application, estimation error always exists for the proposed observers given in Figures 2 and 3, defined as

$$\epsilon_d = \widehat{F}_d - F_d, \tag{26}$$

$$\epsilon_{ai} = F_{ai} - \widehat{F}_{ai}. \tag{27}$$

Consider a Lyapunov candidate function $V = (1/2)ms^2$. Taking the derivative of V and applying (26) and (27) to the resultant equation lead to

$$\begin{aligned}\dot{V} &= sm\dot{s} = s\left(F_a - F_d - m\ddot{x}^* + \beta\dot{e}\right) \\ &= s\left(\sum_{i=1}^{p}\left(\epsilon_{ai} + \widehat{F}_{ai}\right) - \left(\epsilon_d + \widehat{F}_d\right) - m\ddot{x}^* + \beta\dot{e}\right).\end{aligned} \tag{28}$$

From (12) with the controller (21), it can be shown that $F_{ai}^{\mathrm{cmd}} \to \widehat{F}_{ai}$ as the wheel system becomes steady and $\widehat{F}_{ai} \to F_{ai}$; thus, the force control error exists in general, defined as

$$\epsilon_{fi} = \widehat{F}_{ai} - F_{ai}^{\mathrm{cmd}}. \tag{29}$$

Based on which, the function $\dot{V}$ in (28) becomes

$$\begin{aligned}\dot{V} &= s\left[\sum_{i=1}^{p}\left(F_{ai}^{\mathrm{cmd}} + \epsilon_{ai} + \epsilon_{fi}\right) - \left(\widehat{F}_d - \epsilon_d\right) - m\ddot{x}^* + \beta\dot{e}\right] \\ &= s\left(F_a^{\mathrm{cmd}} + \sum_{i=1}^{p}\left(\epsilon_{ai} + \epsilon_{fi}\right) + \epsilon_d - \widehat{F}_d - m\ddot{x}^* + \beta\dot{e}\right)\end{aligned} \tag{30}$$

from which with (20), we get

$$\dot{V} = -k_0 s^2 + s\left[\sum_{i=1}^{p}\left(\epsilon_{ai} + \epsilon_{fi}\right) + \epsilon_d\right]. \tag{31}$$

Note that according to (18), (24), (26), and (27), the estimation errors ϵ_{ai} and ϵ_r can be represented as

$$\begin{aligned}\epsilon_d &= \widehat{F}_d - F_d = -\frac{s}{s+g_d}F_d, \\ \epsilon_{ai} &= F_{ai} - \widehat{F}_{ai} = \frac{s}{s+g_a}F_{ai}\end{aligned} \tag{32}$$

which imply that both ϵ_d and ϵ_{ai} are bounded since the resistance F_d and the adhesive force F_{ai} are continuous or piecewise continuous for practical operation of HSTs, so that the force control error ϵ_{fi} is bounded according to (12) and (21). In other words, there exists a constant ε_0 ensuring

$$\left|\sum_{i=1}^{p}\left(\epsilon_{ai}+\epsilon_{fi}\right)+\epsilon_d\right|<\varepsilon_0<\infty \tag{33}$$

so that $\dot{V}$ given in (31) is bounded as

$$\dot{V}\le -|s|\left(k_0 s-\varepsilon_0\right) \tag{34}$$

which guarantees that the filter error s is confined in the region $|s(t)|\le(1/k_0)\varepsilon_0$ eventually; equivalently, we have $|e(t)|\le(1/\beta k_0)\varepsilon_0$ and $|\dot{e}(t)|\le(2/k_0)\varepsilon_0$ as $t\to\infty$ according to (6); as a result, bounded stable tracking/braking operation is achieved.

Remark 4. This method adopts the same double layered structure as the previous one, and in the upper layer, a disturbance observer is designed to estimate the lumped term F_d (including running resistance and nonlinear in-train effect), so that the adhesive force command can be generated more easily in contrast with most existing methods. However, since the generation of adhesive force commands and adhesive force control is designed independently, the proposed double layered structure as given in (20) and (21) implies that the effect of nonlinear adhesion and wheel dynamics cannot be compensated completely. In view of this, an improved approach is investigated in the next subsection.

3.3. Simplified Observer Based Method. Combining (3) and (12) induces

$$m\ddot{x}=\frac{1}{R}\sum_{i=1}^{p}T_{mi}-\frac{J}{R}\sum_{i=1}^{p}\dot{\omega}_i-F_d\left(\cdot\right) \tag{35}$$

which represents a synthesizing dynamic system including dynamics of the train body and all driving wheels.

It is interesting to note that if the term $F_d(\cdot)$ and accelerations of all driving wheels $(J/R)\sum_{i=1}^{p}\dot{\omega}_i$ are considered as a synthesizing disturbance of the system (35), that is,

$$F_{dw}\left(\cdot\right)=\frac{J}{R}\sum_{i=1}^{p}\dot{\omega}_i+F_d\left(\cdot\right), \tag{36}$$

then the system (35) can be simplified as

$$m\ddot{x}=\frac{1}{R}\sum_{i=1}^{p}T_{mi}-F_{dw}\left(\cdot\right), \tag{37}$$

and the filtered error dynamic system (7) becomes

$$m\dot{s}=\frac{1}{R}\sum_{i=1}^{p}T_{mi}-F_{\mathrm{dis}}\left(\cdot\right)-m\ddot{x}^*+\beta\dot{e}. \tag{38}$$

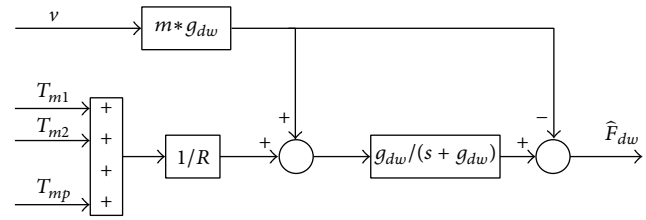

Figure 4: Disturbance observer ($\widehat{F}_{dw}$).

Inspired by above-mentioned methods, a new observer based method can be developed as

$$T_{mi}=\frac{1}{p}\left[-k_0 s+m\ddot{x}^*-\beta\dot{e}+\widehat{F}_{dw}\left(\cdot\right)\right], \tag{39}$$

where the observer is designed as in Figure 4 to indirectly get the synthesizing force term $F_{\mathrm{dis}}(\cdot)$, and from Figure 4 and (37), it is not difficult to verify that

$$\begin{aligned}\widehat{F}_{\mathrm{dis}}&=\frac{g_{dw}}{s+g_{dw}}\left[g_{dw}mv+\frac{1}{R}\sum_{i=1}^{p}T_{mi}\right]-g_{dw}mv\\&=\frac{g_{dw}}{s+g_{dw}}\left[\frac{1}{R}\sum_{i=1}^{p}T_{mi}-m\ddot{x}\right]=\frac{g_{dw}}{s+g_{dw}}F_{\mathrm{dis}},\end{aligned} \tag{40}$$

where $g_{dw}>0$ represents the cutoff frequency of the observer, so that $\widehat{F}_{dw}\to F_{dw}$ is ensured as g_{dw} is larger than the bandwidth of the synthesizing dynamic system (35). Furthermore, it can be shown that bounded stability is achieved by the proposed control, and the tracking errors during traction/braking operation are bounded as $|e(t)|\le(1/\beta k_0)\epsilon_{dw}$ and $|\dot{e}(t)|\le(2/k_0)\epsilon_{dw}$, where ϵ_{dw} represents the upper bound of the estimation error the observer given in Figure 4.

4. Numerical Simulations

To validate the performance of the proposed control strategies, simulation tests are carried out on a train similar to CRH-3 with eight vehicles (i.e., four locomotives and four carriages), and each vehicle includes two bogies and four wheel axles. Considering that a locomotive averagely hauls a carriage, the HST is simplified as a train with two vehicles: one locomotive and one carriage, whose parameters are given as follows: the number of driving wheels $p=4$, average mass of each vehicle $m_i=48$ ton (i.e., total mass $m=2m_i=96$ ton), average axle-load $N_{i0}=m_i g=117.6$ kN, the rotational inertia of a wheel $J=80\,\mathrm{kg\cdot m^2}$, and the wheel radius $R=0.495$ m. Also, unbalanced axle-load is considered in the following simulation, which is represented as $N_i=N_{i0}+\Delta N_i$, where ΔN_i denotes the unbalanced load acted on wheel axle of the locomotive, which is given as $\Delta N_i=(\pm1.5\%, \pm2.5\%)N_{i0}$ for four driving axles, respectively. The train running resistance is modeled as $F_d=0.407+0.2916v+0.0067v^2$.

Suppose that the HST accelerates from 0 km/h to 200 km/h (55.6 m/s) within 200 sec, the rail surface condition changes in the period $50\le t\le100$ sec to reflect the effect of

the rail surface conditions on the proposed control. More specifically, two different adhesive coefficient curves defined by (13)–(15) are given as

IF $50 \le t \le 100$ sec (dry rail)

$$\begin{aligned} b_1 &= 1.786, \quad b_2 = 40.0, \quad b_3 = 10.0, \\ c_1 &= 0.040, \quad c_2 = 3.78, \quad c_3 = 33.3 \end{aligned} \tag{41}$$

ELSE (wet rail)

$$\begin{aligned} b_1 &= 2.046, \quad b_2 = 15.0, \quad b_3 = 10.0, \\ c_1 &= 0.060, \quad c_2 = 12.9, \quad c_3 = 72.2 \end{aligned} \tag{42}$$

END

which represents an usual case; for example, the train enters into and then gets out a tunnel during a raining day.

To verify the effectiveness of the proposed controllers, comparative simulations are implemented by the following four control cases considered.

Case 1. Model based control (MBC):

$$T_{mi} = \frac{R}{p}\left[-k_0 s + m\ddot{x}^* - \beta\dot{e} + F_d(\cdot)\right]. \tag{43}$$

Case 2. MBC + Adhesive force control:

$$\begin{aligned} F_{ai}^{\mathrm{cmd}} &= -\frac{1}{p}\left[-k_0 s + m\ddot{x}^* - \beta\dot{e} + F_d(\cdot)\right], \\ T_{mi} &= k_a\left(F_{ai}^{\mathrm{cmd}} - \widehat{F}_{ai}\right) + \widehat{F}_{ai}R. \end{aligned} \tag{44}$$

Case 3. Double observer based control:

$$\begin{aligned} F_{ai}^{\mathrm{cmd}} &= -\frac{1}{p}\left[-k_0 s + m\ddot{x}^* - \beta\dot{e} + \widehat{F}_d(\cdot)\right], \\ T_{mi} &= k_a\left(F_{ai}^{\mathrm{cmd}} - \widehat{F}_{ai}\right) + \widehat{F}_{ai}R. \end{aligned} \tag{45}$$

Case 4. Simplified observer based control:

$$T_{mi} = \frac{R}{p}\left[-k_0 s + m\ddot{x}^* - \beta\dot{e} + \widehat{F}_{dw}(\cdot)\right], \tag{46}$$

where Case 1 represents an ideal controller when the wheel dynamics is ignored; in Case 2 the adhesive force command F_{ai}^{cmd} is generated by an ideal MBC and then is realized by an observer based force feedback control; in Case 3 the adhesive force command F_{ai}^{cmd} is generated by an observer based controller and then is realized by an observer based force feedback control; in Case 4 the actual control signal T_{mi} is directly designed by using an observer to deal with the running resistance and wheel dynamics; $\widehat{F}_{ai}$, $\widehat{F}_d(\cdot)$, and $\widehat{F}_{dw}$ in the later three cases are estimated from the observers given in Figures 2, 3, and 4, respectively; and control parameters are chosen as $k_0 = 50$, $k_a = 2$, $\beta = 1$, and $g_d = g_{dw} = g_{ai} = 10$.

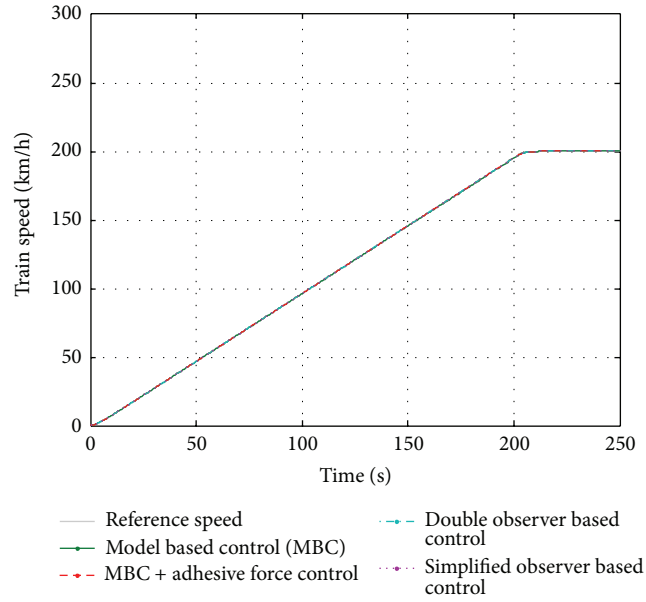

Figure 5: Evolution of the train speed.

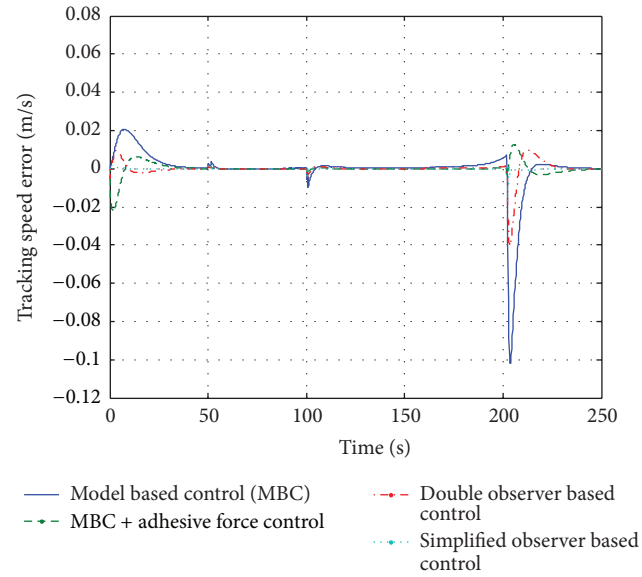

Figure 6: Performance of tracking speed error.

The comparative simulation results are shown in Figures 5–7. Figure 1 shows that the four controllers achieve almost the same tracking performance and all can ensure that the train follows the reference speed precisely. However, small differences still can be observed from Figures 6 and 7, where both speed and position tracking errors of Case 1 without considering wheel dynamics are significantly larger than the other cases (the average position tracking error of Case 1 is about ten times larger than those of the later three cases), which implies that the proposed controllers (i.e., the latter three cases) perform better than the MBC, so that taking the wheel dynamics into account in traction/braking control design of HSTs is effective to improve traction/braking performance for HSTs.

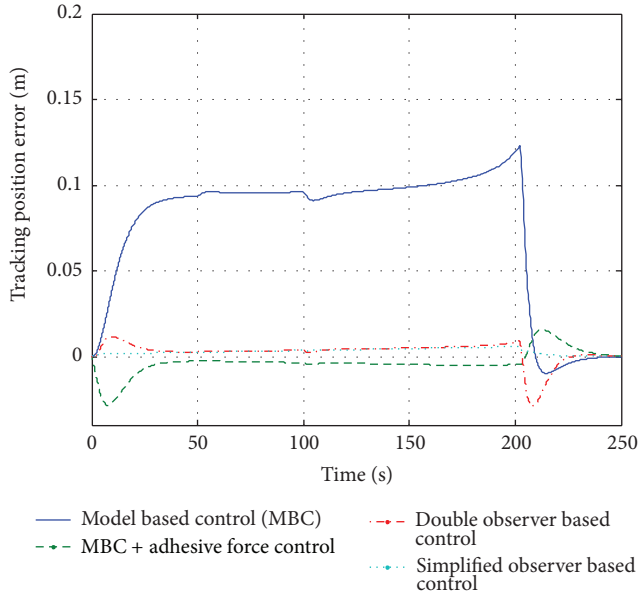

Figure 7: Performance of tracking position error.

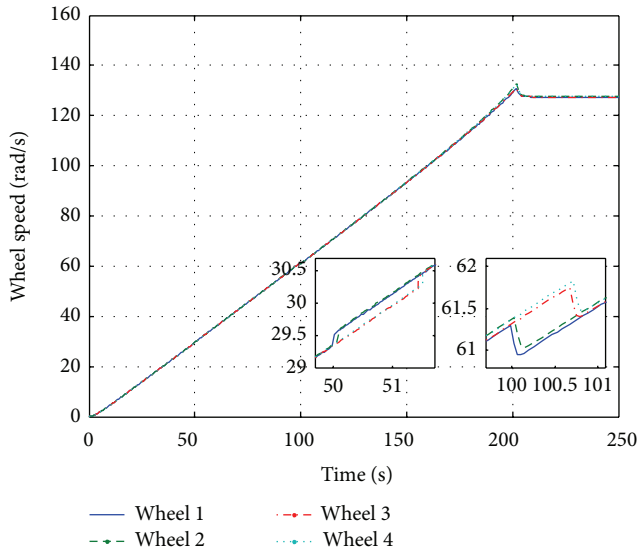

Figure 8: Rotational speed of each driving wheel.

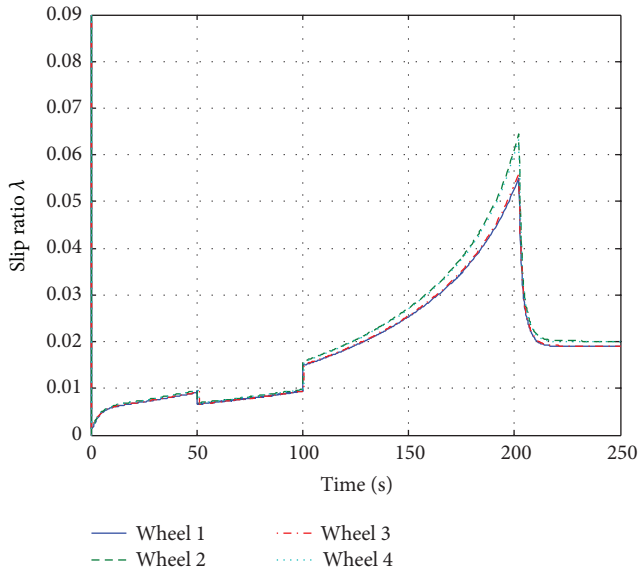

Figure 9: Slip ratio of each driving wheel.

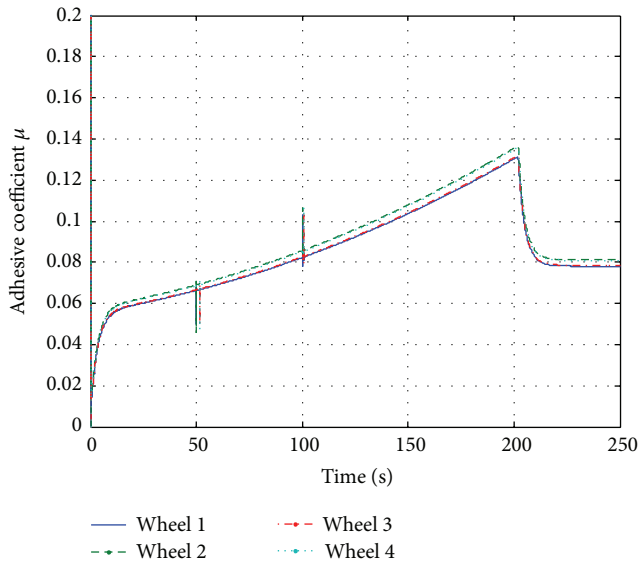

Figure 10: Adhesive coefficient of each driving wheel.

Moreover, differences also exist among the proposed three cases due to different process methods for the wheel dynamics. More specifically, Case 2 performs better than Case 3 because the adhesive force command F_{ai}^{cmd} is generated by an ideal MBC for Case 2, which is more accurate than that supplied by an estimated method. Similarly, Case 4 is better than Case 2 because the wheel dynamics is directly compensated in Case 4, but is only concerned in implementation of F_{ai}^{cmd} and is not considered during generation of F_{ai}^{cmd} in Case 2. Again, this verifies that the wheel dynamics determined by the rail-wheel adhesion conditions is a very important factor affected the control performance of HSTs and thus is necessary to be addressed explicitly during control design.

Note that all above results are achieved under varying rail conditions and unbalanced axle-loads, which lead to different wheel performances. Figures 8–12 show the detailed information of wheel rotational speed, slip ratio, adhesive coefficient, adhesive force, and estimated forces respectively under the control of Case 3 (The other cases have almost the same results; thus, they are not shown here.) The overall rotational speed of driving wheels changes smoothly during the entire operation from Figure 8; that is, only slight changes appear around $t = 50$ s and $t = 100$ s because at those moments the rail changes from wet surface to dry surface and from dry surface to wet surface, respectively. However, from the point view of slip ratios, the small variation of rotational speed of driving wheels significantly changes the wheel-rail adhesion according to Figure 9. In spite of this, the overall adhesive coefficients and actual adhesive force still change smoothly according to Figures 10 and 11, where impulses arise in

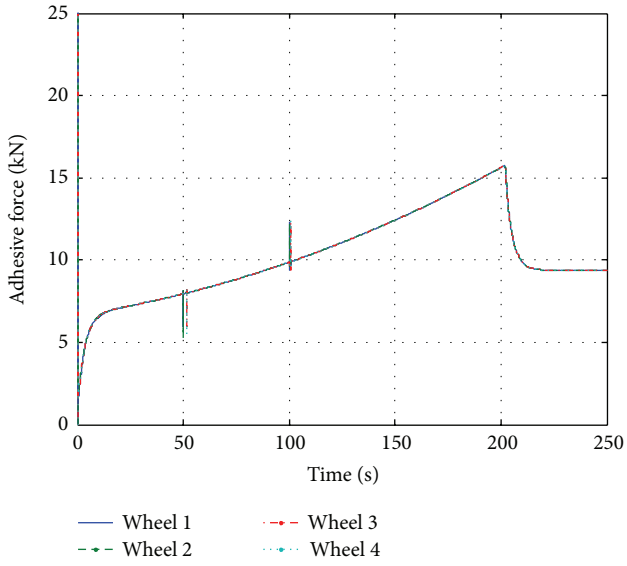

Figure 11: Adhesion force of each driving wheel.

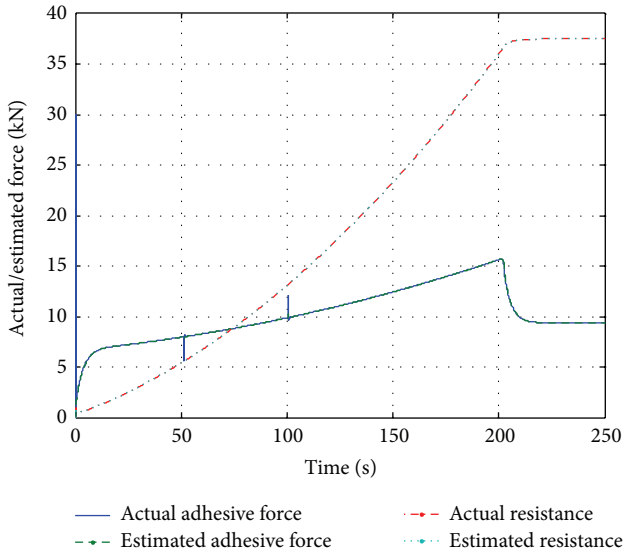

Figure 12: Observer performance.

adhesive coefficients and adhesive force only at the moment that the rail surface sharply changes. This implies that the desired adhesive force can be obtained by the given control since the resistance force and the actual adhesive forces are estimated precisely by the proposed force observers, as shown in Figure 12. Moreover, it is worth mentioning that all these results are achieved under unbalanced axle-loads. Obviously it can be seen that unbalanced axle-loads certainly lead to variation in wheel speed, slip ratio, adhesive coefficient, and so forth, from Figures 8–10; however, the actual adhesive forces are almost the same for different driving wheels, so that balanced driving forces from distributed driving systems are always ensured without considering the actual mass distribution, which is highly desirable for HSTs.

It is important to note that even though the speed and position tracking error of Case 1 are small under the given simulation conditions, they are only achieved by the idea MBC where the complicated lumped term $F_d(\cdot)$ as given (4) is assumed to be available. In other words, if most existing methods are directly applied to practical HSTs' operation without adhesive force control, their tracking performance must become worse than that of Case 1 shown in Figures 6 and 7. Thus, taking complexity and nonlinearities (such as complicated resistances, uncertain and nonlinear wheel-rail adhesion, and driving wheel dynamics) in actual HST systems into account of the proposed control design is necessary and of practical importance, which will significantly improves operation performance of HSTs.

5. Conclusion

It is known that the traction/braking operation depends on the wheel-rail adhesion system. For HSTs, the adhesion coefficient of the HST not only varies with the wheel-rail surface condition, but also changes with the running speed such that under the consideration of actual adhesion conditions, the traction/braking control design of HSTs becomes significantly challenging. In this work, force observers are applied to estimate the unknown and highly nonlinear adhesion force or/and the train running resistance. So based on these force observers, a simple and effective traction/braking control scheme is designed for HSTs. Since the actual adhesion condition is taken into account of control design and the force estimation avoids complicated computation, the proposed traction/braking controller is more feasible and easier to be implemented for real application in contrast with most traction/braking control methods.

Conflict of Interests

The authors declare that there is no conflict of interests regarding the publication of this paper.

Acknowledgments

This work was supported in part by the National Natural Science Foundation of China (nos. 61203124 and 61134001) and the Fundamental Research Funds for the Central Universities (no. 2012JBM009).

References

[1] P. G. Howlett, "The optimal control of a train," *Annals of Operations Research*, vol. 98, pp. 65–87, 2000.

[2] X. Zhuan and X. Xia, "Optimal scheduling and control of heavy haul trains equipped with electronically controlled pneumatic braking systems," *IEEE Transactions on Control Systems Technology*, vol. 15, no. 6, pp. 1159–1166, 2007.

[3] M. Chou and X. Xia, "Optimal cruise control of heavy-haul trains equipped with electronically controlled pneumatic brake systems," *Control Engineering Practice*, vol. 15, no. 5, pp. 511–519, 2007.

[4] C.-D. Yang and Y.-P. Sun, "Mixed H_2/H_∞ cruise controller design for high speed train," *International Journal of Control*, vol. 74, no. 9, pp. 905–920, 2001.

[5] Q. Song, Y.-D. Song, T. Tang, and B. Ning, "Computationally inexpensive tracking control of high-speed trains with traction/braking saturation," *IEEE Transactions on Intelligent Transportation Systems*, vol. 12, no. 4, pp. 1116–1125, 2011.

[6] W. D. Wang and Q. Y. He, "Dynamic problems in high-speed train systems," *Mechanical Programming*, vol. 25, no. 1, pp. 134–143, 1995.

[7] H. Tian, "Study on the characteristics of train air resistance under wind environment," *China Railway Science*, vol. 29, no. 5, pp. 108–112, 2008.

[8] S. Kumarawadu and T.-T. Lee, "Neuroadaptive output tracking of fully autonomous road vehicles with an observer," *IEEE Transactions on Intelligent Transportation Systems*, vol. 10, no. 2, pp. 335–345, 2009.

[9] Q. Song and Y.-D. Song, "Data-based fault-tolerant control of high-speed trains with traction/braking notch nonlinearities and actuator failures," *IEEE Transactions on Neural Networks*, vol. 22, no. 12, pp. 2250–2261, 2011.

[10] Q. Song, Y. D. Song, and W. Cai, "Adaptive backstepping control of train systems with traction/braking dynamics and uncertain resistive forces," *Vehicle System Dynamics*, vol. 49, no. 9, pp. 1441–1454, 2011.

[11] Y. D. Song, Q. Song, and W. C. Cai, "Fault-tolerant adaptive control of high speed trains under traction/braking failures: a virtual parameter based approach," *IEEE Transaction on Intelligent Transportation Systems*, 2013.

[12] M. Spiryagin, K. S. Lee, and H. H. Yoo, "Control system for maximum use of adhesive forces of a railway vehicle in a tractive mode," *Mechanical Systems and Signal Processing*, vol. 22, no. 3, pp. 709–720, 2008.

[13] B. Allotta, E. Melin, A. Ridolfi, and A. Rindi, "Development of an innovative wheel-rail contact model for the analysis of degraded adhesion in railway systems," *Tribology International*, vol. 69, pp. 128–140, 2014.

[14] A. Tesfaye, H. S. Lee, and M. Tomizuka, "A sensitivity optimization approach to design of a disturbance observer in digital motion control systems," *IEEE/ASME Transactions on Mechatronics*, vol. 5, no. 1, pp. 32–38, 2000.

[15] S. Katsura, Y. Matsumoto, and K. Ohnishi, "Modeling of force sensing and validation of disturbance observer for force control," *IEEE Transactions on Industrial Electronics*, vol. 54, no. 1, pp. 530–538, 2007.

[16] S. Katsura, K. Irie, and K. Ohishi, "Wideband force control by position-acceleration integrated disturbance observer," *IEEE Transactions on Industrial Electronics*, vol. 55, no. 4, pp. 1699–1706, 2008.

[17] L. Wang, H. Zhang, and X. Liu, "Sliding mode variable structure I/O feedback linearization design for the speed control of PMSM with load torque observer," *International Journal of Innovative Computing, Information and Control*, vol. 9, no. 8, pp. 3485–3496, 2013.

[18] N. Zaidi, H. Azza, M. Jemli, M. Boussak, and A. Chaari, "DSP implementation of speed vector control for single-phase induction motor based on proportional sliding mode control law," *International Journal of Innovative Computing, Information and Control*, vol. 9, no. 7, pp. 2727–2740, 2013.

[19] X. Su, P. Shi, L. Wu, and Y.-D. Song, "A novel control design on discrete-time takagi-sugeno fuzzy systems with time-varying delays," *IEEE Transactions on Fuzzy Systems*, vol. 20, no. 6, pp. 655–671, 2013.

[20] L. Wu, X. Su, and P. Shi, "Output feedback control of Markovian jump repeated scalar nonlinear systems," *IEEE Transactions on Automatic Control*, vol. 59, no. 1, pp. 199–204, 2014.